Image analysis and in situ FTIR as complementary detection tools for photocatalytic soot oxidation

Image analysis and *in situ* FTIR as complementary detection tools for photocatalytic soot oxidation

Myrthe Van Hal,[1] Sammy W. Verbruggen[1*], Xiao-Yu Yang[2], Silvia Lenaerts,[1] Tom Tytgat[1]

[1] Sustainable Energy, Air & Water Technology (DuEL), Department of Bioscience Engineering, University of Antwerp, Groenenborgerlaan 171, 2020 Antwerp, Belgium

[2] State Key Laboratory of Advanced Technology for Materials Synthesis and Processing, Wuhan University of Technology, 122, Luoshi Road, Wuhan, 430070, China

* Sammy.Verbruggen@uantwerp.be; Groenenborgerlaan 171, 2020 Antwerp, Belgium

Abstract

Air pollution, especially particulate matter (PM), is an increasingly urgent problem in urban environments, causing both short and long-term health problems, climate interference and aesthetical problems due to building fouling. Photocatalysis has been shown to be a possible solution to that end. In this work two complementary detection methods for photocatalytic soot oxidation are studied and their advantages and disadvantages are discussed.

First, a colour-based digital image analysis method is drastically improved towards an accurate, detailed and straightforward detection tool, that enables simultaneous measurement of the degradation of different grades of soot fouling (for instance a shallow soot haze *versus* condensed soot deposits). In the next part, a second soot oxidation detection method is presented based on *in situ* FTIR spectroscopy. This method has the additional advantage of providing more insight into the photocatalytic soot degradation process by monitoring both gaseous and adsorbed intermediates as well as reaction products while the reactions are ongoing.

As an illustration, the proposed detection strategies were applied on four different commercially available and synthesized photocatalytic materials. The digital image analysis showed that P25 (Evonik) is the fastest photocatalytic soot degrader of all studied materials for both a uniform soot haze as well as concentrated soot spots. Application of the *in situ* method showed that for all studied materials

adsorbed formate-related surface species were formed and that commercially available ZnO nanopowder has the highest specificity towards complete mineralization into CO_2.

With this we aim to provide a set of complementary experimental tools for the convenient, reliable, realistic and standardised detection of photocatalytic soot degradation.

Keywords

Photocatalytic soot oxidation, Digital image analysis, *In situ* FTIR, Titanium dioxide, Zinc oxide

1. Introduction

Air pollution is a current challenge that globally affects human health and the environment. In urban environments particulate matter (PM) is one of the most important pollutants, often exceeding the World Health Organization (WHO) Air Quality annual mean target for PM_{10} and $PM_{2.5}$ (respectively 20 and 10 μg/m³).[1,2] PM can originate from a variety of sources, although in urban environments it is mostly caused by combustion processes.[1] Long-term exposure to PM is known to cause a variety of health problems (e.g. respiratory diseases, cardiovascular disease) and in addition, PM has recently also been linked to many other negative health effects such as low birth weight, preterm birth, DNA damage and mutagenic activity, cardiovascular diseases etc.[3,4] In addition, PM also has an influence on the global climate both increasing (e.g. black carbon) and decreasing (e.g. SO_4^{2-}, NH_4^+) the global temperature.[1,5] Next to health and environmental effects PM also causes buildings to deteriorate due to fouling.[6] An important component of PM is soot, which is mainly composed of elemental carbon and carbon-based organic matter.[1]

Research has shown the potential of photocatalysis for soot degradation.[7–12] The photocatalyst is activated when light strikes the material with a photon energy larger than the bandgap energy of the photocatalyst, resulting in the generation of electron-hole pairs. The holes can be used in oxidation

reactions and can in this way be utilized for the degradation of organic pollutants including soot. Photocatalytic soot degradation using TiO_2 has first been shown by Lee and Choi in 2002. They were able to completely oxidize the bulk of a 2 µm layer of soot towards CO_2 after 30 h of irradiation. In this study $OH^{\bullet}$ radicals were assigned as the main oxidant species, however, they also acknowledged the necessity of the presence of oxygen to enable photocatalytic soot oxidation.[8]

The limited amount of literature available on the topic of photocatalytic soot oxidation mainly deals with aspects of self-cleaning applications, mechanistic considerations and kinetic modelling of the overall reaction.[7–10,13–16] Although photocatalytic soot oxidation is a tough reaction, and involves various practical difficulties, little research has been done on the development and improvement of user-friendly and unambiguous soot oxidation detection methods.[12] This is important to gain better insight into the process of photocatalytic soot degradation, but it also facilitates and improves the photocatalyst screening for a given application.

The detection method developed by Smits *et al.* (2013) relies on the colour change of a soot-covered photocatalyst layer using digital image analysis.[12] This method has the advantage over the conventionally used quartz crystal microbalance that it is cheap and less time-consuming since multiple samples can be analysed simultaneously. The method also has some important drawbacks. A first drawback is the use of a threshold value to classify each pixel in the digital image as either fouled with soot or completely clean, without any intermediate classification. This is not a realistic interpretation of the soot degradation process and thus may lead to misinterpretations. As soot is degraded, the colour of each pixel gradually shifts from fouled (black) to clean (original colour), over intermediate (grey) values. In this work the digital analysis method is drastically improved by determining the grade of fouling of each pixel. By doing so, the aforementioned problem is circumvented, and it is now possible to get a more realistic, complete view on the degradation of soot and in addition simultaneously study the degradation of different grades of soot fouling. This improvement was validated by comparison with absorbance measurements.

Two remaining drawbacks of this digital image analysis are (i) its use being restricted to white photocatalysts (given the fact that it is a method relying solely on colour change), and (ii) that it provides no data whatsoever on the reaction products and thus ongoing reaction pathways. To deal with these final limitations an *in situ* FTIR detection method is studied, based on a reaction cell introduced by Hauchecorne *et al.* in 2011.[17] The cell enables to probe the photocatalytic surface as well as the surrounding gas phase simultaneously, while the irradiation process is ongoing. Complementary information on both gaseous reaction products and adsorbed intermediate surface species can thus be obtained in a single measurement.

To evaluate the proposed detection methods the photocatalytic soot oxidation capability of common photocatalytic materials (TiO_2, ZnO) was studied, which was by our knowledge the first time for ZnO.

2. Experimental

2.1. Material synthesis

The ZnO nanoparticles were synthesized according to a precipitation method described by Chen *et al.* (2016).[18] A sol-gel synthesis method was used to synthesize nano-sized TiO_2 according to Qiu *et al.* (2006).[19] The formed yellow crystals were calcined at 600°C for 3 hours to obtain a combination of anatase and rutile crystal phases. A combination of both crystalline phases often results in a higher activity, as is the case for the commercially available P25.[20] Commercially available photocatalysts P25 and ZnO nanopowder (< 100 nm) were purchased from Evonik and Sigma Aldrich, respectively, and used as received. These materials were used as such in all further experiments.

2.2. Photocatalyst coating

Soda lime glass slides (2.5x1.5 cm^2, VWR) were washed in Piranha solution (70% sulfuric acid (H_2SO_4, Chem-Lab, 95-97%), 30% hydrogen peroxide (H_2O_2, ChemLab)) for 30 minutes. The photocatalytic materials were suspended in methanol (Merck) by sonication for 1 hour (66.7 mg mL^{-1}). Application of the coating was performed by drop casting the suspension on a dry glass slide, resulting in a photocatalyst loading of 3.56 mg cm^{-2}. The glass slides were then dried in air at room temperature for 2 hours and subsequently overnight at 80°C. As a model compound for soot black carbon (Printex-U, Evonik) was suspended in methanol by sonication for 1 hour (1 mg mL^{-1}). This solution was drop casted on the coated glass slides (0.022 mg cm^{-2}). The glass slides were again dried for 2 hours at room temperature and overnight at 80°C. Finally, the glass slides were placed in a vacuum furnace for 2.5 hours at 35°C.

2.3. Physical characterization

UV-VIS absorbance spectra of the samples were recorded using a Shimadzu UV-2600 spectrophotometer with integrating sphere. Barium sulfate ($BaSO_4$) was used as reference. Using the Tauc-plot method the band gap (Eg) of the different photocatalytic materials was determined.

The specific surface area of the synthesized materials was determined by a N_2-adsorption/desorption measurement (Micrometrics - Tristar 3000). The samples were pre-treated for 24 h at 200°C under continuous N_2 purging and measurements were performed using N_2 at -196°C.

Atomic force microscopy (AFM) measurements (Bruker Dimension Edge) were performed at a scan range of 2 µm and a scan rate of 0.5 Hz to determine the surface morphology of the photocatalysts.

X-ray diffraction (XRD) was used to characterize the structure and crystallinity of the synthesized powders using a Bruker D8 Advance diffractometer with Cu $K\alpha$ radiation (40 kV, 40 mA). The scan ranged from 20-80 degrees applying a scan rate of 0.5 s $step^{-1}$.

2.4. Colour-based monitoring of photocatalytic soot oxidation

A soot-fouled surface obviously darkens when more soot is being deposited. In this way, the result can be directly related to the contemporary problem of fouling of buildings, resulting in aesthetical deterioration. The extent of photocatalytic soot degradation can be monitored by quantifying the discolouration of the surface using digital images, as was suggested by Smits et al. (2013).[12] In this work this method will be significantly improved towards a more accurate and complete soot oxidation detection method. In addition, a second detection method also based on visual soot degradation will be used for validation purposes. The experiments were all performed by positioning the samples 3 cm under a Philips fluorescence S 25 W UVA lamp, resulting in an incident light intensity of 2.1 mW cm^{-2} in the region of 290 till 400 nm (λ_{max} at 354 nm), as measured by a calibrated spectroradiometer (Avantes Avaspec-3648-USB2).

Pictures were taken in a standardized photobox,[12] excluding external light and direct illumination. A Canon Eos 500D camera was positioned 20 cm above the samples and the digital images were taken in manual mode (iso 200, aperture f8 and focal exposure 1:5) at maximal resolution (5184 x 3456) at 72 dpi. The digital images were processed using the image software ImageJ in the CIELAB colour space. For all digital image analysis experiments the entire glass slide sample area (1.5x2.5 cm^2) was studied. The L* coordinate was used as a measure of the amount of soot deposition (brightness axis) and ranged between 0 (black) and +100 (white). Rather than pre-defining a threshold value to categorize a pixel as either fouled with soot or completely clean, the adaptation suggested in this study is to use the shift of the most frequent L* value (measured in the majority of the pixels) as a measure for soot degradation. In this way, soot degradation can be visualized and observed when the pixels become brighter, resulting in a shift of most frequent L* value towards higher (i.e. 'whiter') L* values. This results in a more realistic representation of the cleaning of the surface. An additional advantage of this improved method is that by considering all L* values, a distinction can be made between different grades of soot fouling, thus allowing to simultaneously monitor the degradation of different grades of soot fouling (e.g. a shallow soot haze *versus* condensed soot spots).

In Experiment 1 each photocatalyst was applied onto four glass slides. Three glass slides were illuminated, one was kept in the dark as negative control. Photographs were taken from the glass slides before and after soot deposition at specific UV illumination intervals (e.g. 0, 16, 24, 48, 120, 288, 504, 672, 984 and 1560 hours). The obtained pictures were processed in ImageJ to determine the frequency of the L* values. In order to compare the photocatalytic soot degradation of different photocatalytic materials the shift in most frequent L* value was expressed relative to the most frequent L* value of a completely fouled glass slide (L_0). The relative soot degradation efficiency of a uniform soot haze can in this way be expressed as in (Eq. 1) and is shown in Figure 1a:

$$\textit{Degradation efficiency uniform soot haze (\%) = Rel Lmax (\%)} = \frac{L_b}{L_a} \cdot 100 = \frac{L_t - L_0}{L_0 - L_{NS}} \cdot 100 \qquad \text{(Eq.1)}$$

Where L_t is the position of the most frequent L* value at a specific time of irradiation, L_0 is the position of the most frequent L* value at the beginning of the experiment (no UV illumination = completely fouled glass slide) and L_{NS} is the position of the most frequent L* value when no soot has been deposited on the photocatalyst yet (clean glass slide).

The relative degradation efficiency of concentrated soot spots can be determined by the 'height' (number of pixels) of the peak relative to the peak height of a completely fouled glass slide (NP_0) (eq. 2) and is illustrated in Figure 1b:

$$\textit{Degradation efficiency concentrated soot spots (\%) = Rel NPmax (\%)} = \frac{NP_b}{NP_a} \cdot 100 = \frac{NP_0 - NP_t}{NP_0 - NP_{NS}} \cdot 100 \qquad \text{(Eq.2)}$$

Where NP_t is the height of the concentrated soot peak at a specific time of irradiation, NP_0 is the height of this peak at the beginning of the experiment (no UV illumination = completely fouled glass slide) and NP_{NS} is the height of this peak when no soot has been deposited on the photocatalyst yet (clean glass slide).

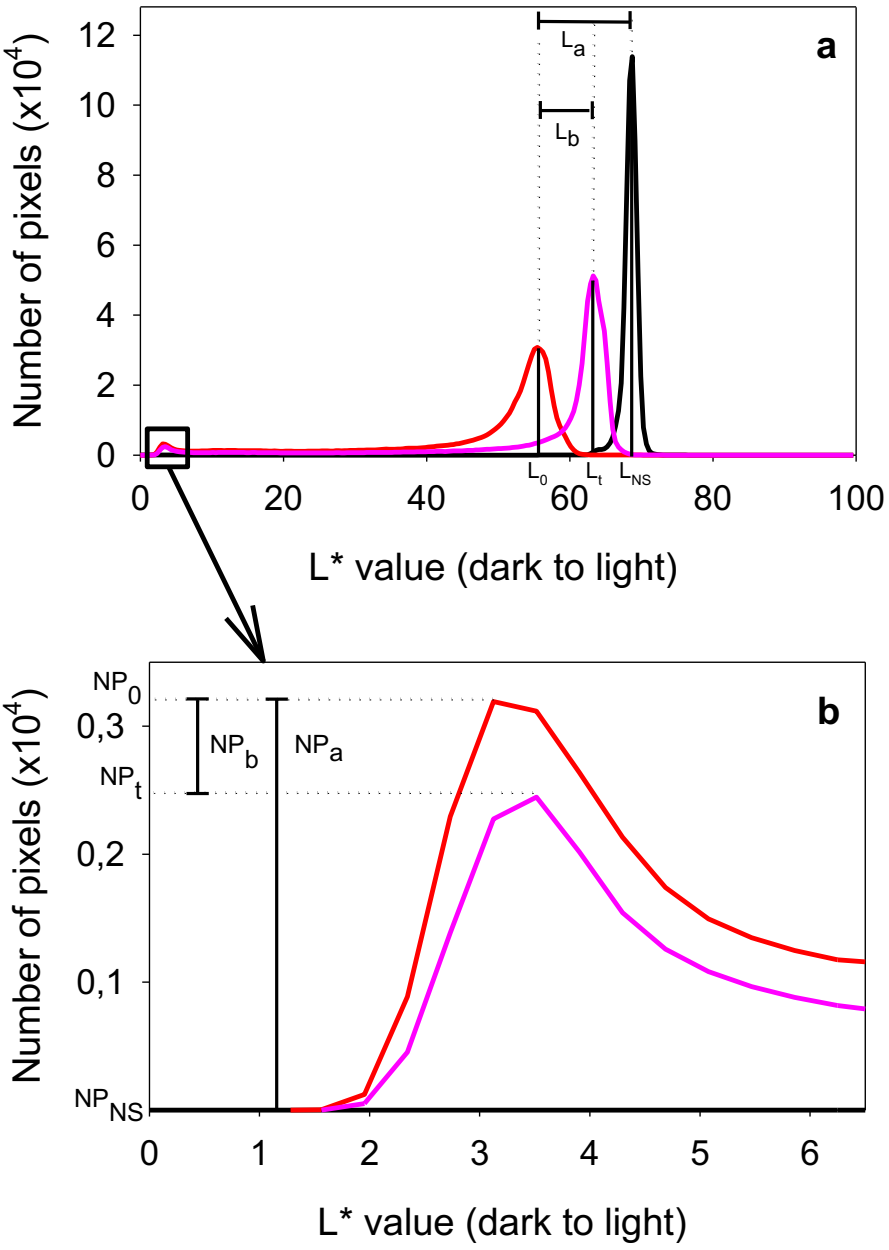

Figure 1. a) Illustration of determination of the soot degradation efficiency of a uniform soot haze using the improved digital image analysis with the result before soot deposition (black), before UV illumination (red) and after 120 h of UV illumination (pink) b) Illustration of determination of the soot degradation efficiency of concentrated soot spots using the improved digital image analysis with the results before soot deposition (black), before UV illumination (red) and after 120 h of UV illumination (pink).

Corrections for possible deviations caused by small changes in the background illumination were made by processing a set area of the background in ImageJ and applying the hereby obtained deviation in L* value to the complete dataset of that time point.

To validate the improvements made to the digital image analysis method suggested by Smits et al. (2013),[12] a second optical detection method (absorbance method) was used to measure the photocatalytic soot degradation. The results obtained by this absorbance method could then be compared with the results obtained with both the original and the improved digital image analysis. In Experiment 2 the coated glass slides were again illuminated using a UVA lamp. Photographs were taken at specific UV illumination time intervals (e.g. 0, 16, 24, 48, 120, 288, 504, 672 and 984 hours) and in addition the absorbance of each glass slide was measured each time. This colorimetric method is based on the decrease in absorbance of the samples when soot is being degraded. For this colorimetric analysis an AvaSpec-3648-USB2 spectroradiometer was used. The samples were placed in the standardised photobox during the absorbance measurements.[12] The complete absorbance spectrum in the visible range (400-700 nm) was measured, however, since the shape of the absorbance spectra was the same for all measurements, as shown in Supporting info Fig. S1, only the absorbance value at 600 nm was used. To quantify the soot degradation using the obtained absorbance values, the absorbance at 600 nm was divided by the initial absorbance at this wavelength, resulting in the value A_t/A_0 representing the amount of fouling on the surface. To compare these results with the results obtained with the digital image analysis, the results were expressed as (Eq. 3):

$$\textit{Degradation efficiency uniform soot haze (\%)} = \left(1 - \frac{A_t}{A_0}\right).100 \quad \text{(Eq.3)}$$

2.5. I*n situ* monitoring of photocatalytic soot oxidation

Insight into the photocatalytic activity at the catalyst surface was gathered using a patented *in situ* Fourier Transform infrared (FTIR) reaction cell designed by Hauchecorne *et al.* (2011). The experimental details on the cell design can be retrieved from reference [17]. Printex-U was used as a model compound for soot. To achieve a round flat pellet, 5 mg of a mixture containing the photocatalyst powder and 0.6 wt% soot (Printex-U) was thoroughly mixed with 115 mg KBr (VWR) and pressed for 2 minutes at 5 tons. This pellet was placed in the centre of the *in situ* reaction cell. Before starting the measurement, the reactor was flushed with air at 200 mL min^{-1} until a stable readout was

obtained.[21] Next, the reactor was sealed airtight and the batch experiment was started. Over a period of 12 hours, the pellet was illuminated by eight UV LEDs at each side placed in a circular pattern (10 mW each, Roithner LaserTechnik) with an incident intensity of 330 μW cm^{-2} in the region of 350 till 420 nm (λ_{max} at 377 nm). This was followed by a 2-hour control measurement without illumination to confirm the air tightness of the reactor.

3. Results and discussion

3.1. Characterisation

The obtained characteristics of the photocatalyst powders used in this study are summarized in Table 1. It is clear that the BET surface area of P25 and the synthesized TiO_2 are similar, however, the synthesized ZnO results in a significant increase in surface area compared to the commercially available form. The adsorption isotherms (Supporting info Fig. S2) clearly show that both ZnO materials are non-porous. P25, as also known from literature, is also non-porous,[22] although agglomerates lead to some macroporous interparticle pores. TiO_2 synthesized according to Qiu *et al.* (2006) on the other hand is characterised by a mesoporous structure. In addition, it can be seen that the band gaps of the synthesized materials are similar to the commercial ones for both TiO_2 and ZnO. Using AFM measurements, the roughness of the photocatalyst layers was determined. From the AFM surface maps (Fig. S3) it can be concluded that all four photocatalyst layers can be considered as very rough, since they are all simple powder films. Based on the root mean square values (Table 1) both commercial materials (P25 and ZnO_{Sigma}) form a somewhat less rough layer compared to the materials that were synthesized in the lab, with the least rough surface for P25. Overall, it should be clear that such films are not suitable for practical implementation, but in the scope of the present study on photocatalytic soot detection methods this inhomogeneity does not appear to be a decisive factor.

Table 1. Characteristics of commercial and synthesized materials as powder films on glass

Material	Bandgap Eg (eV)[3]	Surface area BET ($m^2 g^{-1}$)	Surface roughness (Rq) (µm)	Crystallite particle size (nm)[4]
$P25_{Evonik}$[1]	3.2	52	0.026	19 (A)[5], 32 (R)[5]
$TiO_{2\ Qiu,\ 2006}$[2]	3.1	68	0.128	30 (A)[5], 36 (R)[5]
$ZnO_{Sigma\ Aldrich}$[1]	3.3	11	0.053	<100[6]
$ZnO_{Chen,\ 2016}$[2]	3.3	49	0.112	17

1) commercially available photocatalysts
2) Photocatalysts synthesized based on literature protocols
3) Obtained by the Tauc method applied on diffuse reflectance spectra
4) Estimated from XRD using the Scherrer equation
5) A= anatase, R=rutile
6) According to manufacturer data (Sigma-Aldrich)

The structure and crystallinity of the synthesized materials was determined using X-ray diffraction (Figure 2). The TiO_2 sample was calcined for 3 hours at 600°C to obtain a combination of the crystalline forms anatase and rutile, which is confirmed by the XRD pattern in Figure 2a. In Figure 2b the characteristic XRD pattern for the hexagonal wurtzite structure of ZnO can be observed.

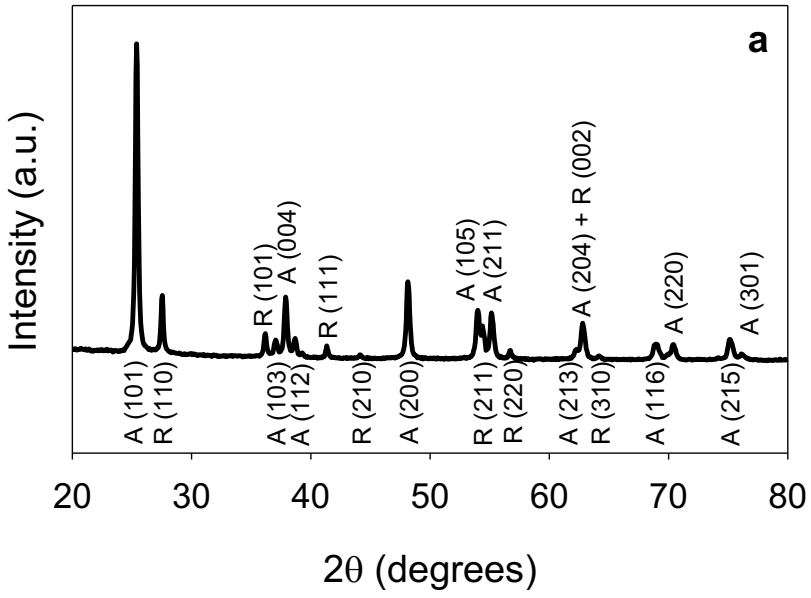

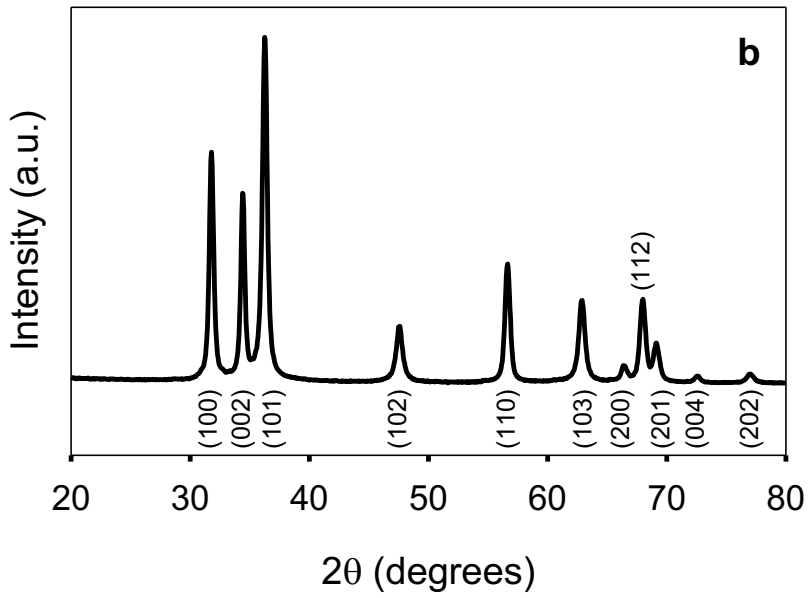

Figure 2. XRD pattern of a) TiO_2 synthesized according to Qiu et al. (2006) after calcination for 3 h at 600°C b) ZnO synthesized according to Chen et al. (2016), which were used in all described experiments.

3.2. Colour-based monitoring of photocatalytic soot oxidation

In the first part of this study the original digital image analysis method was drastically improved towards more accurate and detailed monitoring of (photocatalytic) soot degradation. This is done by using the shift of the most frequent L* value (the brightness axis of the CIELab colour space) as a measure for visual soot degradation instead of using a fixed threshold value to categorize each pixel as either fouled or clean. When a soot haze is degraded, the most frequent L* value is expected to shift towards higher and thus brighter L* values.

In Experiment 1 (see Section 2.4) the coated glass slides were illuminated with UV light and digital images were taken at specified time intervals. The result for P25 is shown in Figure 3a. At 0h the sample is dark grey, which changes over light grey towards the original colour of the coated glass slides (left) when soot is completely photocatalytically degraded. When applying the described improved method, a graph plotting the number of pixels against the L* value can be obtained, resulting in Figure 3b for

P25. On this graph the photocatalytic soot degradation observed in Figure 3a is reflected by the shift of the most frequent L* value towards higher L* values. This shift of the most frequent L* value can then be expressed as a soot degradation efficiency using (Eq. 1), resulting in Figure 3c for P25. In addition, it can be observed from Figure 3b that next to the shift in the peak, also its shape changes when soot is photocatalytically degraded. Initially, a broad low peak is present, reflecting the large amount of different dark grey tones on a completely fouled glass slide. When soot is degraded all pixels shift towards higher ('whiter') L* values and more and more pixels will have similar 'whiter' colours, resulting in more pixels with the same L* value and thus a higher narrower peak.

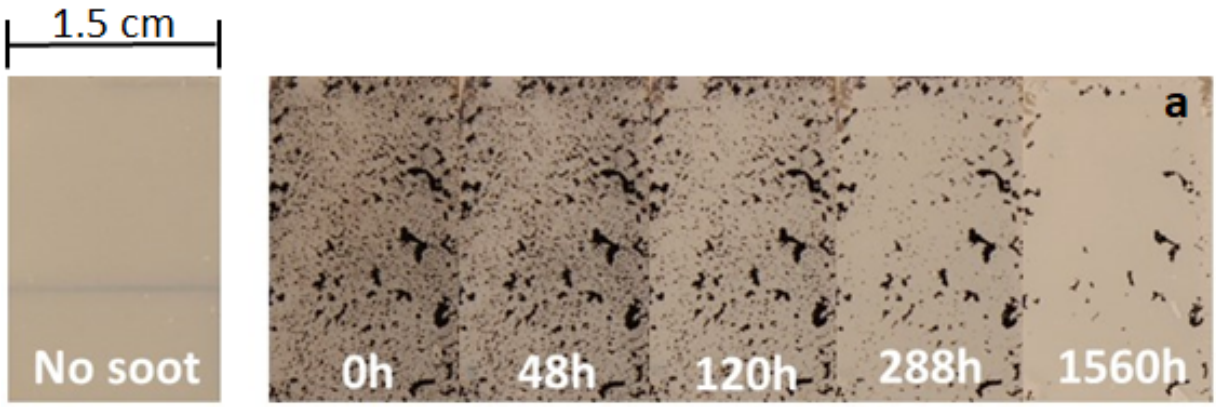

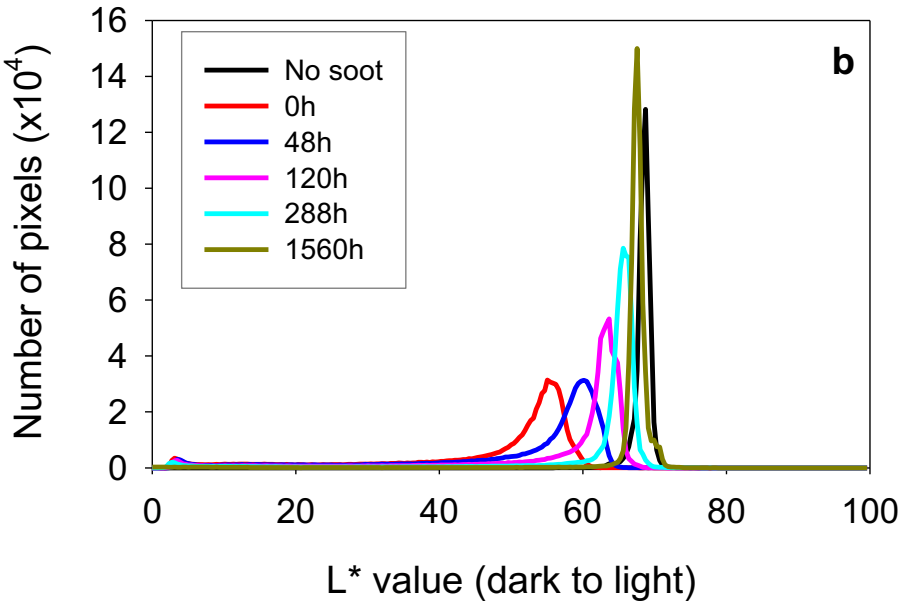

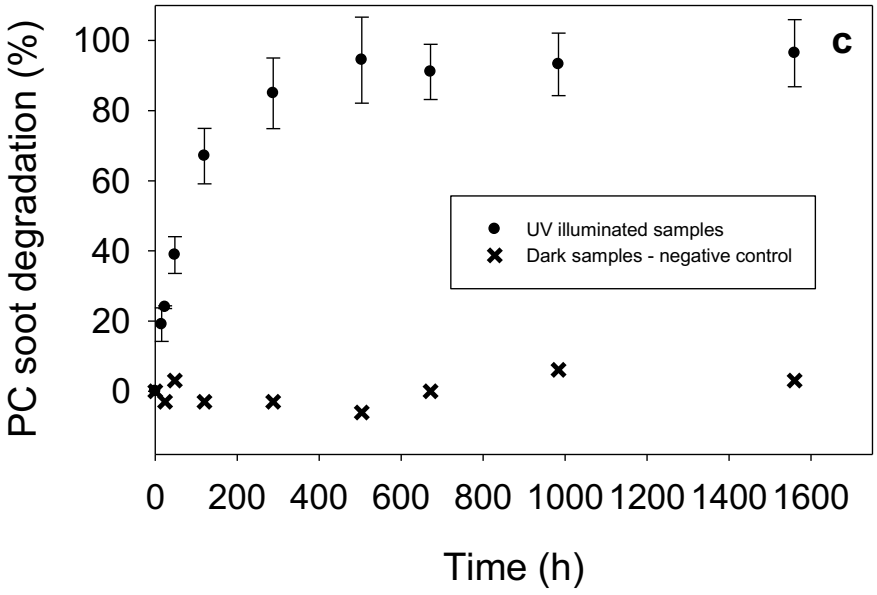

Figure 3. Experiment 1: a) Subsequent digital images of the photocatalytic soot degradation on a glass slide coated with P25 with f.l.t.r. a glass slide without soot, with soot before UV illumination, after 48, 120, 288 and 1560 hours of illumination. b) Number of pixels plotted against the L value, representing the degradation of a uniform soot haze by P25. c) Photocatalytic soot degradation of uniform soot haze (expressed as relative L*max) by P25, as a function of UV illumination time. The error bars are based on three samples.*

The here presented improved method allows to visualise the degradation of soot as a shift in most frequent L* value, resulting in a more detailed view on the soot degradation process. It is clear from Figure 3a that a distinction can be made between different gradations of soot fouling, that are not all completely degraded at the same time. From Figure 3c it can be seen that for P25 complete soot degradation is reached after 984h, however, some concentrated soot spots can still be observed at that time (Figure 3a). As Figure 3c is based on the shift of the peak that is originally present at a L* value of 69 (Figure 3b), this specifically applies to the 'haze' of soot that is deposited uniformly over the glass slide. However, at the left of Figure 3b a second small peak can be observed at low L* values, reflecting the presence of concentrated black soot spots, and is shown in more detail in Figure 4a. It is clear from Figure 4a that these soot spots are also degraded over time, although slower, visualised by the decreasing height of this peak. This illustrates the main limitation of the technique: since it is a visual method, soot oxidation can only be detected when the colour of the surface changes significantly. Thus, when a very thick layer of soot would be present, it is possible that soot is already being oxidised without any visual colour change at that particular location. When the concentrated

soot spots are substantially degraded they will no longer contribute to the presence of concentrated soot spots (e.g. disappearance of small L* peak at low L* values) but instead contribute to the haze. The presented adaptation thus enables to separately quantify the degradation of these concentrated soot spots (Eq. 2), which was not possible in the original method. It can be concluded that the suggested adaptations thus result in more realistic and detailed data.

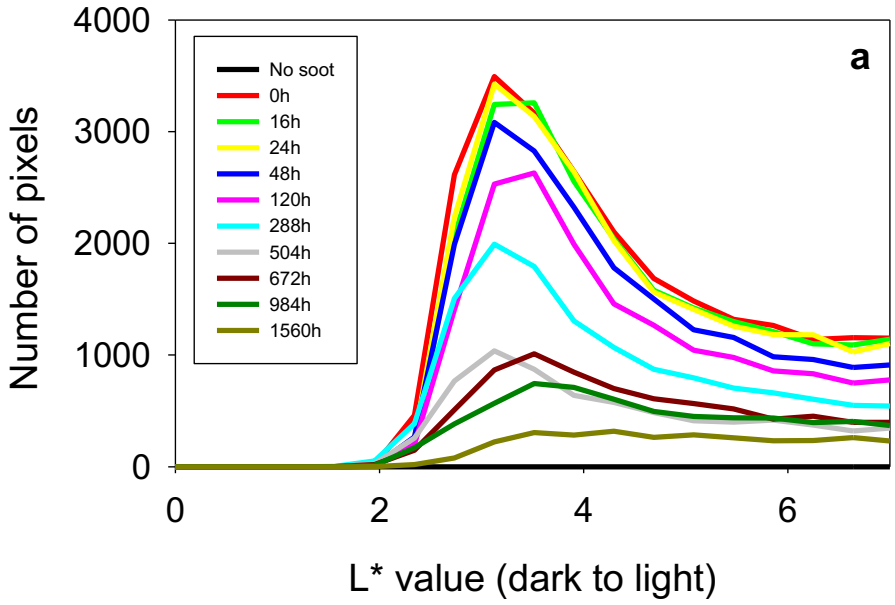

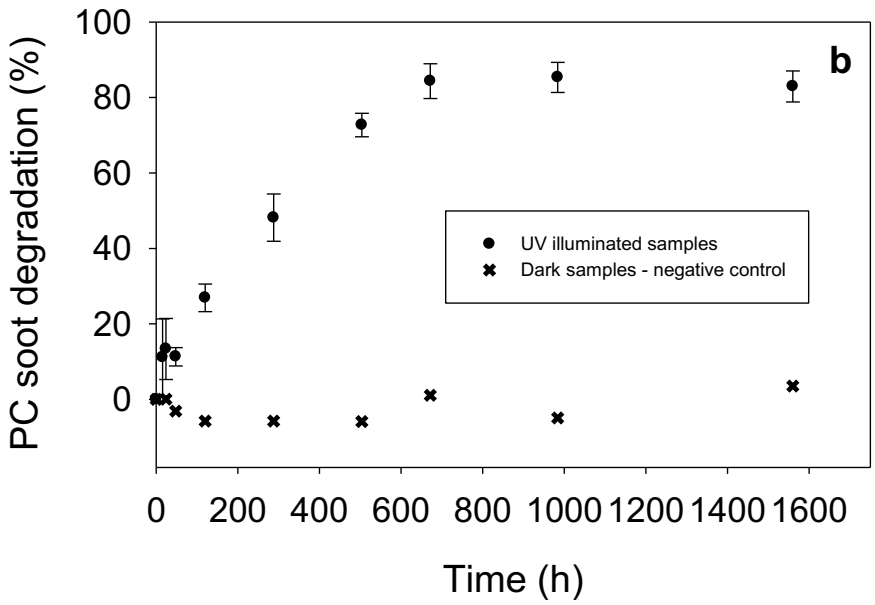

Figure 4. Experiment 1: a) Number of pixels plotted against the L value for P25, representing the photocatalytic degradation of concentrated soot spots. b) Photocatalytic soot degradation of concentrated soot spots (expressed as relative NPmax) by P25, as a function of UV illumination time.*

The accuracy of the proposed method is validated by comparing the results obtained with both the original and the improved digital image analysis with a second colour-based soot oxidation detection method. This second method is based on the decreasing absorbance of a soot fouled surface when soot is being degraded. This validation experiment (Experiment 2) is presented in Figure 5a, demonstrating that the results obtained by the absorbance method and the improved digital image analysis are in good agreement. When applying the method as described by Smits et al. using a single fixed threshold value for L*,[12] it can be seen from Figure 5a that large differences exist with the results obtained by the absorbance method. The threshold value depends on a variety of parameters, such as the substrate (e.g. mortar samples *versus* glass slides), the colour of the coating, the light source/intensity in the pictures, etc. and should thus be separately determined for each experiment. Thus when using the original digital image analysis a calibration with a different detection method is always needed to determine the threshold value. As the improved digital image analysis directly reflects the actual amount of soot degradation independent of a threshold value this is a much more

generic and straightforward method for the detection of soot degradation. Also in the study of Smits et al. (2013) a discrepancy between the results obtained with the original digital image analysis and those generated by the absorbance method was present as both methods clearly gave different results for all intermediate time points. [12] This also reflects the unrealistic representation of soot degradation when using a single threshold value, as the colour of a soot fouled surface will not instantly change from black to white when soot is degraded but will rather brighten slowly over time, running over several grey tones.

Given all the above, it is therefore clear that the suggested adaptations indeed result in a more accurate, realistic, reliable and straightforward detection tool, that also enables to simultaneously detect the degradation of concentrated soot spots, which was not possible before.

The effect of the studied area on the accuracy of the results was determined by applying the improved digital image analysis on a five times smaller area of the glass slide for P25 (see Supporting info Fig. S4). For a soot haze it is clear from Fig. S4 that the results obtained by studying a smaller area of the glass slide are very similar to those obtained when analysing the entire glass slide (average deviation is only 0.8%). For the concentrated soot spots a good agreement between both results can be observed with an average deviation of 6%. Thus, it can be concluded that the improved digital image analysis is not very sensitive to the study area, but to obtain the most accurate results for the degradation of concentrated soot spots it is advised to use a large enough study area (at least 1 cm^2).

As a proof-of-concept study the adapted digital image analysis is applied to assess the soot degradation capacity (haze) of four photocatalytic materials using the two described colour-based methods (Figure 5b). In the Supporting info (Fig. S5) these results were again compared with the results of the original digital image analysis showing large deviations with the absorbance method. In addition, the photocatalytic degradation of concentrated soot spots was simultaneously monitored with the improved digital image analysis and is presented in Figure 5c.

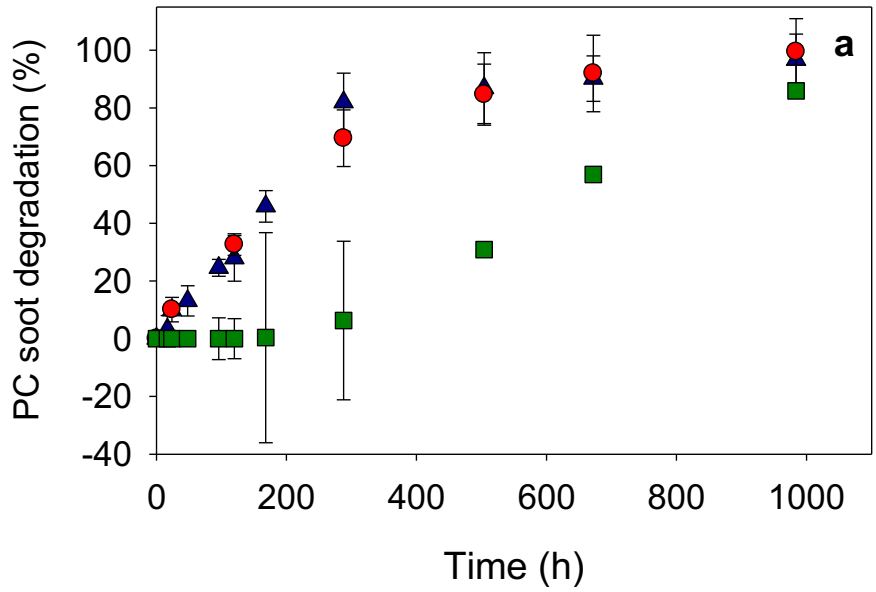
a
PC soot degradation (%)
100
80
60
40
20
0
-20
-40
0
200
400
600
800
1000
Time (h)

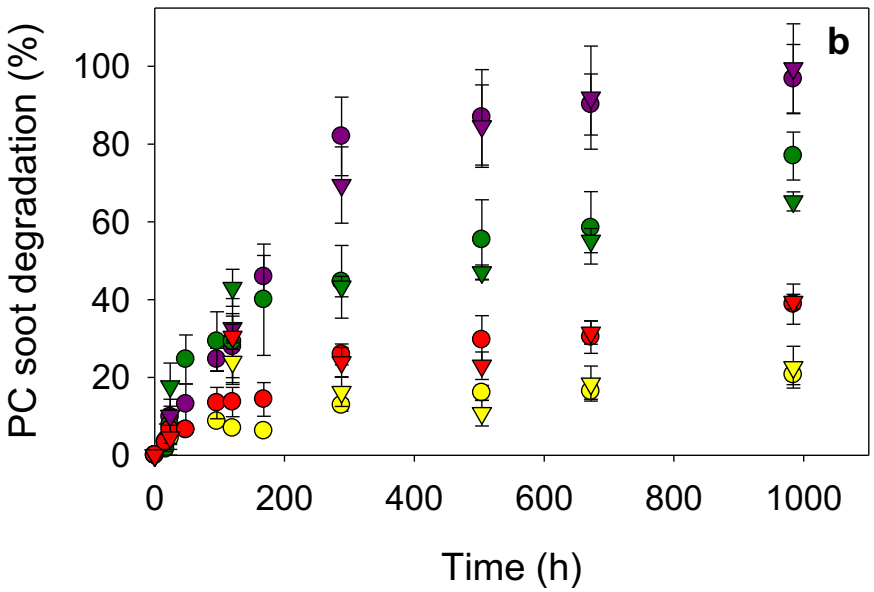
b
PC soot degradation (%)
100
80
60
40
20
0
0
200
400
600
800
1000
Time (h)

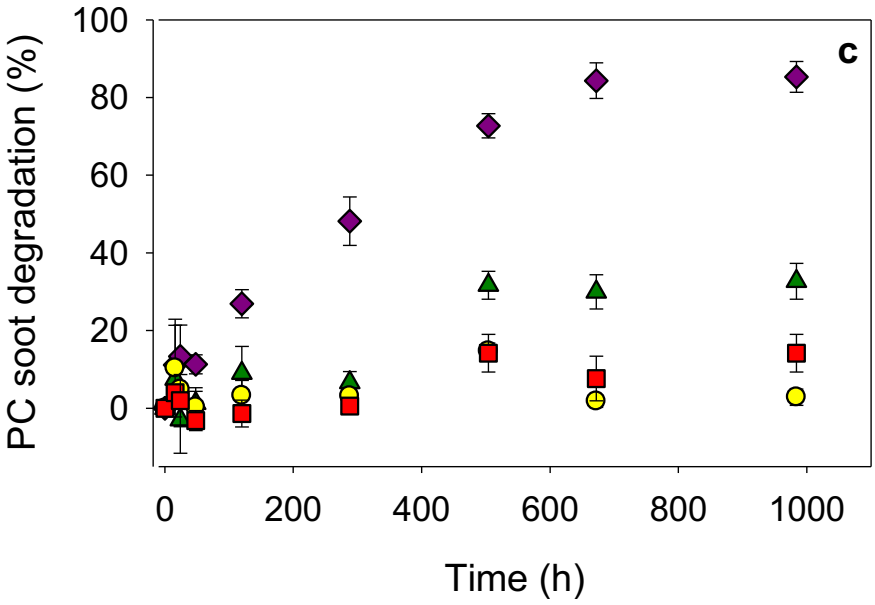

Figure 5. Experiment 2: a) Photocatalytic soot degradation by P25 in function of UV illumination time: comparison of absorbance method (red ●), the original digital image analysis (green ■) and the improved digital image analysis (blue ▲). b) Photocatalytic soot degradation of uniform soot haze by P25 (purple), $TiO_{2\ Qiu,\ 2006}$ (green), $ZnO_{Chen,\ 2016}$ (red) and ZnO_{Sigma} (yellow), in function of UV illumination time: comparison of absorbance (▼) and improved digital image analysis (●). c) Photocatalytic degradation of concentrated soot spots by P25 (purple ◆), $TiO_{2\ Qiu,\ 2006}$ (green ▲), $ZnO_{Chen,\ 2016}$ (red ■) and ZnO_{Sigma} (yellow ●) determined with the improved digital image analysis, as a function of UV illumination time.

Figure 5b clearly shows that P25 is the fastest photocatalytic soot degrader of all studied materials, resulting in complete soot degradation after 41 days (982h) of UV illumination (25 W Philips lamp at 3 cm resulting in an incident irradiance of 2.1 mW cm^{-2}). The TiO_2 synthesized according to Qiu *et al.* (2006) showed a slightly lower soot degradation efficiency, resulting in 65-75% degradation after 41 days. The synthesized and commercial ZnO resulted in a soot degradation efficiency of 39-39.5 and 20.5-22% after 41 days, respectively, illustrating the lower capability of ZnO to degrade soot compared to TiO_2.

Luttrell et al. (2014) illustrated the thickness dependency of the photocatalytic soot oxidation reaction up to a thickness in the range of the diffusion length of the excited carriers as there is only negligible penetration of the soot into TiO_2 layers.[23] From the picture without soot deposition in Figure 3a it can already be observed that the photocatalyst layers used in these experiments are thicker and differences in the photocatalytic soot oxidation rate between the different materials will likely not

originate from different layer thicknesses. As direct oxidation of soot has shown to be the most important oxidation mechanism,[8] all parameters concerning the direct contact area of the photocatalyst with the soot are of key importance for the soot degradation rate. The BET surface area of both TiO_2 forms and $ZnO_{Chen,2016}$ were similar, but the BET surface area of ZnO_{Sigma} was significantly lower (Table 1). The low photocatalytic soot oxidation rate of ZnO_{Sigma} might thus be in part be explained by its low surface area.[24] The better performance of both TiO_2 forms might also be partially explained by the fact that TiO_2 synthesized according to Qiu *et al.* (2006) and P25 showed (meso/macro-) porosity, whereas both ZnO materials where non-porous. The high performance of P25 can also be attributed to its optimal anatase:rutile ratio. From the AFM surface maps it could already be concluded that all four photocatalyst layers can be considered as rough films, which can be ascribed to the fact that they are simply dropcasted powder films. As can be observed in Figure 3a, the deposited soot layer is also inhomogeneous and rough as soot spots are scattered across the surface of the photocatalyst. Therefore, the surface roughness is not likely to be the decisive factor for explaining differences in reactivity within this particular sample set.

For P25, the absorbance is halved in the first 168 h (7 days) of illumination, however, complete soot degradation is only reached after 984 h (41 days), illustrating the fast initial soot degradation resembling first order kinetics. This was also observed in previous studies on photocatalytic soot degradation [7,12,16] and kinetic models have been proposed to that end.[12,13] The same can also be observed for all other studied materials, however, no complete soot oxidation was reached after 41 days of illumination for these materials. A dark experiment was simultaneously performed confirming the absence of soot degradation when the glass slides were not illuminated with UV light.

The degradation of concentrated soot spots can only be monitored using the digital image analysis and the result is shown in Figure 5c. P25 showed around 85% soot spot degradation after 41 days, $TiO_{2\ Qiu,\ 2006}$ gave 33% degradation, $ZnO_{Chen,\ 2016}$ about 10% and ZnO_{Sigma} resulted in about 3% soot degradation after 41 days. For P25, the degradation of the concentrated soot spots largely corresponds to the

degradation of the uniform soot haze (Figure 5b), albeit at a lower rate, which corresponds to what can be observed from Figure 3a. For all the other materials, no to very little soot is being degraded during the first 12 days. Only after 21 days a larger fraction of the soot spots is being visually degraded. This might be explained by the fact that the degradation can initially not be observed on the digital images as the soot spots are still completely black due to the large remaining soot fraction. As P25 has the highest soot degradation capacity of the four studied materials, degradation of the soot spots is visible for P25 earlier.

3.3. *In situ* monitoring of photocatalytic soot oxidation

An important limitation of the two previously described colour-based detection methods is that they only represent the visual result of the soot degradation at a specific time but yield no insight into the occurring reactions over time. Therefore, a second soot oxidation detection method is presented in this study. With this method soot degradation is studied in an FTIR *in situ* reaction cell. This method enables to determine the degradation of soot by the amount of CO_2 that is formed in the airtight reactor. In addition, this method also allows detecting all products formed during photocatalytic soot degradation, both gases as well as adsorbed intermediates at the surface.

In the absence of soot, blank tests demonstrated that no CO_2 evolution can be observed when solely irradiating the KBr-photocatalyst pellets (Supporting info Fig. S6). When such pellets also contain soot, a clear signal corresponding to CO_2 evolution can be measured in the wavenumber range 2290-2390 cm^{-1} (ν_{as}(O=C=O)), as shown in Figure 6. Initially the height of the CO_2 band increased exponentially, after 10 h this increase started to flatten (Supporting info Fig. S7). This flattening was attributed to oxygen depletion in the airtight reaction cell. When the reactor was flushed again with air after CO_2 saturation, the remaining soot could again be further mineralised to CO_2, supporting this hypothesis. In addition, a second important band can be observed in the region 1273-1445 cm^{-1} with two maxima at 1360 (ν_s(COO)) and 1380 cm^{-1} (δ(CH)), that can be attributed to adsorbed formate, $CHOO^-_{(ad)}$.[25] Other bands originating from this compound are possibly masked by steric hindrance, as the observed

formate is bound to the surface of the pellet (Figure 6). The formation of $CHOO^-_{(ad)}$ supports the theory of Chin *et al.* (2009) that soot can be sequentially oxidized towards CO_2 over several intermediates, next to the possibility of direct oxidation towards CO_2. Using EPR and FTIR, the reaction mechanisms described by Chin *et al.* have already been elucidated in more detail.[15] A variety of adsorbed intermediates has been determined, possibly containing C-O-C stretching in anhydrides, aryl ether linkages, aromatic rings, C-O bonds and C-H bonds adsorbed on the surface. In addition, in Figure 6 two negative bands are observed around 2848 and 2922 cm^{-1}, which can be attributed to the disappearance of C-H stretching vibrations and thus provide clear evidence of soot degradation. This C-H band decreases exponentially, stabilising after ca. 10 hours, in agreement with the CO_2 evolution. Carbon monoxide (CO) could not be detected during the reaction. When analysing the FTIR spectra of the three other studied materials the same bands and trends were observed, pointing at similar reaction mechanisms for photocatalytic soot degradation by TiO_2 and ZnO (see Supporting info Fig. S8 for spectra). The production of CO_2 and formate-related species in function of UV illumination time for all four studied materials is shown in Figure 7.

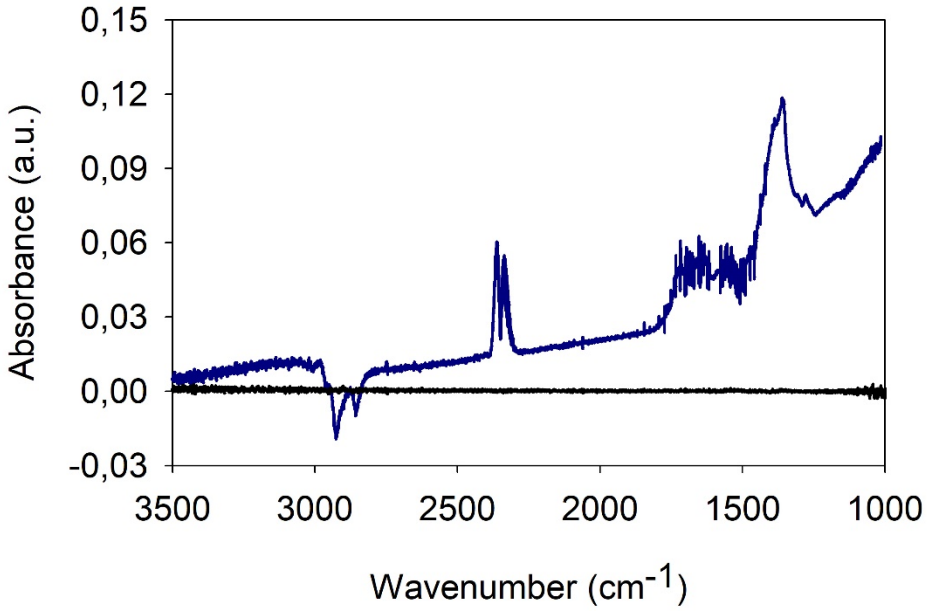

Figure 6. FTIR spectra of KBr-P25-soot pellet in in situ *reactor at start experiment (black) and after 10 hours of UV illumination (blue). Positive bands represent formed products, negative bands point at the degradation of products.*

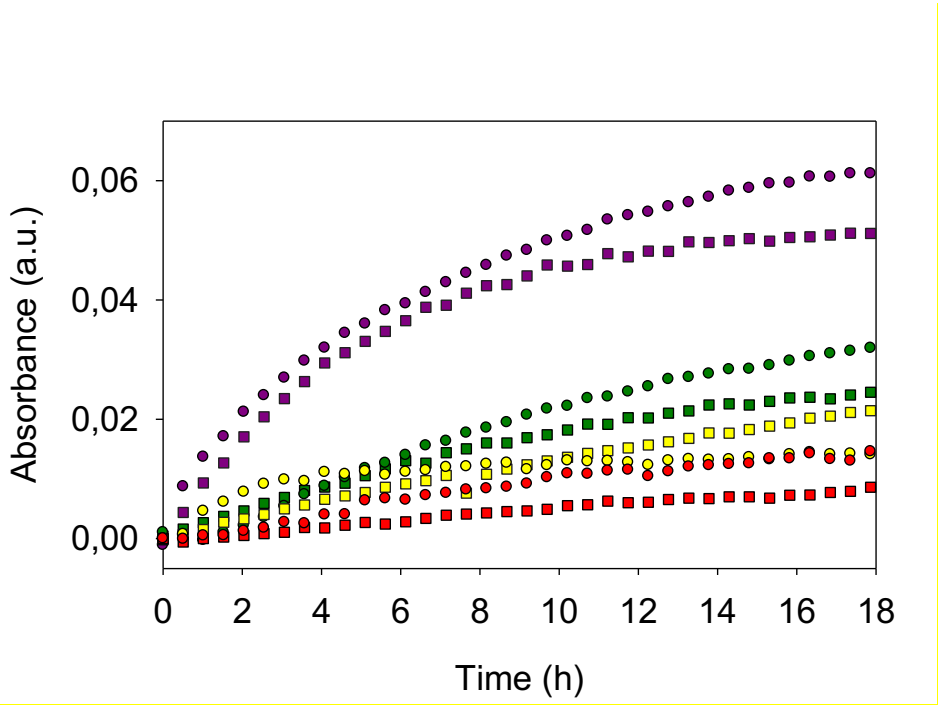

Figure 7. Evolution of CO_2 (■) and formate-related species (●) as a function of UV illumination time for a KBr-photocatalyst-soot pellet placed in the in situ *reactor for following photocatalysts: P25 (purple), $TiO_{2\ Qiu,\ 2006}$ (green), ZnO_{Sigma} (yellow) and $ZnO_{Chen,2016}$ (red).*

By monitoring the CO_2 band at 2360 cm^{-1} during the photocatalytic soot degradation (every half hour, see Supporting info Fig. S7), the soot mineralisation rate could be determined from the initial slope of the CO_2 evolution curve (< 10h).

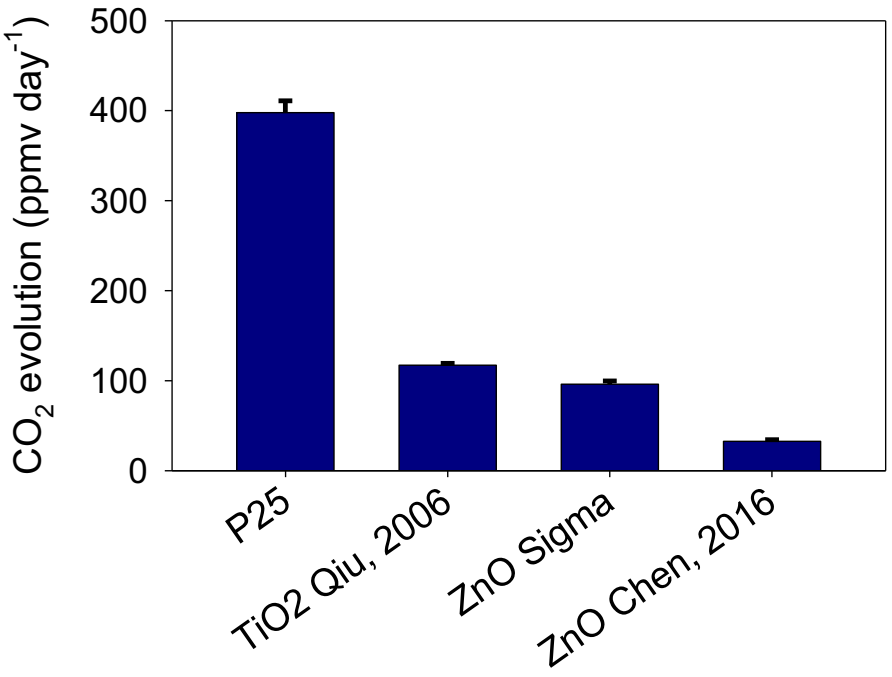

Figure 8. CO_2 evolution of studied materials based on the in-situ soot oxidation detection method.

From Figure 8 it can be observed that the initial mineralisation rate is by far the highest for P25. The three other materials show drastically lower soot mineralisation rates, with $TiO_{2\ Qiu,\ 2006}$ followed closely by ZnO_{Sigma} and the lowest rate for $ZnO_{Chen,\ 2016}$. It is hard to directly compare these results with the colour-based methods, as different substrates were used (glass vs. KBr pellet) and the colour-based methods reflect a visual change, which might not be directly proportional to CO_2 formation. As is clear from Figure 6, CO_2 is not the only product being formed during photocatalytic soot degradation. Therefore, this *in situ* method allows to assess which materials have a high specificity towards CO_2 and thus result in more complete soot degradation after 10 hours of UV illumination. The ratio of the absorbance of CO_2 (2360 cm^{-1}) to formate (1360 cm^{-1}) (after 10 h) is shown in Table 2. These values should solely be used to mutually compare samples, and do not reflect the ratio of actually produced concentrations. From this, ZnO_{Sigma} actually appears to have the highest specificity towards CO_2, followed by P25, $TiO_{2\ Qiu,2006}$ and finally $ZnO_{Chen,\ 2016}$. The discrepancy between the low CO_2 production rate of $ZnO_{Chen,\ 2016}$ determined with the *in situ* technique (Figure 8) and the relatively higher soot

degradation efficiency (compared to ZnO_{Sigma}) measured with the improved digital image analysis can be explained by Table 2. The soot oxidation reaction by $ZnO_{Sigma,\ 2016}$ is more complete than that by $ZnO_{Chen,\ 2016}$ that yields more of the intermediate product formate instead of CO_2.

Table 2. Absorbance ratio of CO_2 to formate for the four studied photocatalysts.

	Ratio of absorbance of CO_2 to formate
P25	0,81
$TiO_{2\ Qiu,2006}$	0,71
ZnO_{Sigma}	1,00
$ZnO_{Chen,\ 2016}$	0,46

Overall, this third *in situ* detection method thus allows monitoring all formed products, both gases and adsorbed intermediates, in *quasi* real-time, which can be regarded a clear benefit over the colour-based analysis methods described above. The only drawback is that dedicated lab equipment is required to that end, whereas the colorimetric methods are more straightforward and image processing can even be done using digital image analysis freeware.

4. Conclusion

In this study two complementary detection methods for soot oxidation were studied. First the digital image analysis suggested by Smits *et al.* (2013) was improved towards a more realistic, accurate, and detailed method.[12] This was achieved by using the shift of the most frequent L* value (CIELab colour space) as measure for visual soot degradation instead of using a fixed threshold value to categorize each pixel as either fouled or clean. The improved digital image analysis was validated by comparison with the absorbance method. The adaptation enables simultaneous measurement of the degradation of different grades of soot fouling. By applying this method we could evidence that P25 is the fastest photocatalytic soot degrader of all studied materials for both a uniform soot haze as well as for concentrated soot spots, followed by $TiO_{2\ Qiu,2006}$, $ZnO_{Chen,\ 2016}$ and finally ZnO_{Sigma}.

In the second part of this study, a second detection method was suggested based on *in situ* FTIR measurements. This method delivers additional insight into the products formed during photocatalytic

soot degradation by monitoring both gaseous and adsorbed reaction products. Using this method, it was shown that for all studied materials $CHOO^-_{(ad)}$ was formed, supporting the hypothesis of Chin *et al.* (2007) of an indirect soot oxidation pathway via solid intermediates, next to direct soot oxidation to CO_2.[13] Using this method, an initial CO_2 production rate could be determined for the studied materials, which was the highest for P25. In addition, using the ratio CO_2 to formate it could be concluded that ZnO_{Sigma} has the highest specificity towards CO_2, followed by P25, $TiO_{2\ Qiu,2006}$ and finally $ZnO_{Chen,\ 2016}$. A more in-depth mechanistic study on the photocatalytic soot oxidation pathways is needed to further increase the insight into the process of photocatalytic soot oxidation.

In conclusion, this study results in a complete detection strategy for soot oxidation that provides a realistic, accurate and all-inclusive description of this photocatalytic process.

5. Acknowledgement

M.V.H. acknowledges the Research Foundation–Flanders (FWO) for a doctoral fellowship. M.V.H., S.W.V., S.L. and X-Y.Y. thank the FWO and the National Natural Science Foundation of China (NSFC) for funding an international collaboration project. Mr. M. Minjauw is greatly thanked for his help in the AFM measurements.

6. Competing interests

The authors declare no competing interests.

7. References

[1] EEA, Air quality in Europe — 2016 report, 2016.

[2] A. van Donkelaar, R. V. Martin, M. Brauer, R. Kahn, R. Levy, C. Verduzco, P.J. Villeneuve, Global estimates of ambient fine particulate matter concentrations from satellite-based aerosol optical depth: Development and application, Environ. Health Perspect. 118 (2010) 847–855. doi:10.1289/ehp.0901623.

[3] A. Mukherjee, M. Agrawal, World air particulate matter: sources, distribution and health effects, Environ. Chem. Lett. 15 (2017) 283–309. doi:10.1007/s10311-017-0611-9.

[4] I.M. Kennedy, The health effects of combustion-generated aerosols, Proc. Combust. Inst. 31 II (2007) 2757–2770. doi:10.1016/j.proci.2006.08.116.
[5] R. deRichter, S. Caillol, Fighting global warming: The potential of photocatalysis against CO2, CH4, N2O, CFCs, tropospheric O3, BC and other major contributors to climate change, J. Photochem. Photobiol. C Photochem. Rev. 12 (2011) 1–19. doi:10.1016/j.jphotochemrev.2011.05.002.
[6] A. Maury, N. De Belie, State of the art of TiO2 containing cementitious materials: self-cleaning properties, Mater. Construcción. 60 (2010) 33–50. doi:10.3989/mc.2010.48408.
[7] A. Mills, J. Wang, M. Crow, Photocatalytic oxidation of soot by P25 TiO2 films, Chemosphere. 64 (2006) 1032–1035. doi:10.1016/j.chemosphere.2006.01.077.
[8] M.C. Lee, W. Choi, Solid phase photocatalytic reaction on the Soot/TiO2 interface: The role of migrating OH radicals, J. Phys. Chem. B. 106 (2002) 11818–11822. doi:10.1021/jp026617f.
[9] S.K. Lee, S. McIntyre, A. Mills, Visible illustration of the direct, lateral and remote photocatalytic destruction of soot by titania, J. Photochem. Photobiol. A Chem. 162 (2004) 203–206. doi:10.1016/j.nainr.2003.07.002.
[10] P. Chin, C.S. Grant, D.F. Ollis, Quantitative photocatalyzed soot oxidation on titanium dioxide, Appl. Catal. B Environ. 87 (2009) 220–229. doi:10.1016/j.apcatb.2008.09.020.
[11] Y. Kameya, K. Torii, S. Hirai, M. Kaviany, Photocatalytic soot oxidation on TiO 2 microstructured substrate, Chem. Eng. J. 327 (2017) 831–837. doi:10.1016/j.cej.2017.06.094.
[12] M. Smits, C. kit Chan, T. Tytgat, B. Craeye, N. Costarramone, S. Lacombe, S. Lenaerts, Photocatalytic degradation of soot deposition: Self-cleaning effect on titanium dioxide coated cementitious materials, Chem. Eng. J. 222 (2013) 411–418. doi:10.1016/j.cej.2013.02.089.
[13] P. Chin, G.W. Roberts, D.F. Ollis, Kinetic Modeling of Photocatalyzed Soot Oxidation on Titanium Dioxide Thin Films, Ind. Eng. Chem. Res. 46 (2007) 7598–7604. doi:10.1021/ie070083t.
[14] B. Bassou, N. Guilhaume, K. Lombaert, C. Mirodatos, D. Bianchi, Experimental microkinetic approach of the catalytic oxidation of diesel soot by ceria using temperature-programmed experiments. Part 2: Kinetic modeling of the impact of the ceria/soot contacts on the rate of oxidation, Energy and Fuels. 24 (2010) 4781–4792. doi:10.1021/ef100582w.
[15] M. Smits, Y. Ling, S. Lenaerts, S. Van Doorslaer, Photocatalytic removal of soot: Unravelling of the reaction mechanism by EPR and in situ FTIR spectroscopy, ChemPhysChem. 13 (2012) 4251–4257. doi:10.1002/cphc.201200674.
[16] M. Smits, D. Huygh, B. Craeye, S. Lenaerts, Effect of process parameters on the photocatalytic soot degradation on self-cleaning cementitious materials, Catal. Today. 230 (2014) 250–255. doi:10.1016/j.cattod.2013.10.001.
[17] B.M.J. Hauchecorne, D.G.M. Terrens, F.J.G. Vanpachtenbeke, S.K. Lenaerts, T. Tytgat, Reaction chamber for studying a solid-gas interaction, 2011.
[18] X. Chen, Y. Li, X. Pan, D. Cortie, X. Huang, Z. Yi, Photocatalytic oxidation of methane over silver decorated zinc oxide nanocatalysts, Nat. Commun. 7 (2016) 12273. doi:10.1038/ncomms12273.
[19] S. Qiu, S.J. Kalita, Synthesis, processing and characterization of nanocrystalline titanium dioxide, Mater. Sci. Eng. A. 435–436 (2006) 327–332. doi:10.1016/j.msea.2006.07.062.
[20] D.C. Hurum, A.G. Agrios, K.A. Gray, T. Rajh, M.C. Thurnauer, Explaining the Enhanced Photocatalytic Activity of Degussa P25 Mixed-Phase TiO 2 Using EPR, (2003) 4545–4549.
[21] T. Tytgat, B. Hauchecorne, M. Smits, S.W. Verbruggen, S. Lenaerts, Concept and validation of a fully automated photocatalytic test setup, J. Lab. Autom. 17 (2012) 134–143. doi:10.1177/2211068211424554.
[22] K.J.A. Raj, B. Viswanathan, Effect of surface area , pore volume and particle size of P25 titania on the phase transformation of anatase to rutile, 48 (2009) 1378–1382.
[23] T. Luttrell, S. Halpegamage, J. Tao, A. Kramer, E. Sutter, M. Batzill, Why is anatase a better photocatalyst TiO 2 films, Sci. Rep. 4 (2014) 1–8. doi:10.1038/srep04043.
[24] S.W. Verbruggen, TiO2 photocatalysis for the degradation of pollutants in gas phase: From morphological design to plasmonic enhancement, J. Photochem. Photobiol. C Photochem. Rev.

24 (2015) 64–82. doi:10.1016/j.jphotochemrev.2015.07.001.
[25] B. Hauchecorne, D. Terrens, S. Verbruggen, J.A. Martens, H. Van Langenhove, K. Demeestere, S. Lenaerts, Elucidating the photocatalytic degradation pathway of acetaldehyde: An FTIR in situ study under atmospheric conditions, Appl. Catal. B Environ. 106 (2011) 630–638. doi:10.1016/j.apcatb.2011.06.026.